PROCEEDINGS, 47th Workshop on Geothermal Reservoir Engineering
Stanford University, Stanford, California, February 7-9, 2022
SGP-TR-223

Cement Formulations for Super-Critical Geothermal Wells

Toshifumi Sugama[1], Tatiana Pyatina[1]

[1]Brookhaven National Laboratory

734 Brookhaven Ave. Upton, NY 11973

tpyatina@bnl.gov

Keywords: geothermal well cement, super-critical wells, TEST-CEM

ABSTRACT

This work is a part of a joint international effort to develop "sustainable geothermal well cement for challenging thermo-mechanical conditions" (Test-Cem) under the umbrella of Cofund GEOTHERMICA. The paper describes an exploratory study of cementitious composites for applications in geothermal wells under super-critical conditions. Preliminary screening of a wide range of blends was done on formulations mixed at room temperature, cured under hydrothermal conditions at 85°C (overnight) followed by overnight hydrothermal curing at 300°C and the final curing under the super-critical conditions at 400°C and pressure of 25.5 MPa (3,700 psi). The tested formulations included high-temperature Portland cement modified with silica ($CaO-SiO_2$ system), P_2O_5-Na_2O-CaO-Al_2O_3-SiO_2 – based systems with varied Al/Si ratios, and P_2O_5-Na_2O-CaO-Al_2O_3-SiO_2-Fe_2O_3 phosphate systems, Na_2O-CaO-Al_2O_3-SiO_2-MgO-Fe_2O_3 and Na_2O-CaO-Al_2O_3-SiO_2-MgO Mg-containing systems, and Na_2O-Al_2O_3-SiO_2 cement system.

Mechanical properties of the blends and crystalline phase transitions were determined after the initial curing and exposure to the super-critical conditions to understand effect of phase transitions upon materials performance. Formulations with short-term compressive strength development of no less than 6.9 MPa (1,000 psi) and stable phase compositions were identified for further testing to fully evaluate their true potential.

1. INTRODUCTION

Very high temperature (>400°C) geothermal wells could provide competitive power at potentially $20-35 per megawatt-hour (MWh)[1]. Currently most geothermal plants rely on concentrated heat located near the surface producing globally only 15 gigawatts (GW). Development and exploitation of super-critical wells may increase energy production by 10 times per well over conventional geothermal and 4-5 times more energy per well than typical shale gas fields[2]. Several worldwide projects have already demonstrated a possibility of reaching super-hot conditions and hot wells potential for power production. They include Iceland Deep Drilling Project[3], Newberry Super-Hot Rock project[4], Japan Beyond Brittle project[5–7], Italy's Larderello geothermal field DESCRAMBLE project[8–11], New Zealand Hotter and Deeper project[12].

One of the necessary components for the construction of hot-temperature wells are materials that can survive under the well conditions. Cements that provide zonal isolation, well structure support, corrosion protection of metallic casing must be designed for temperatures above about 300°C typical for current well cements. So far, the work on high-temperature cementitious materials included characterization of non-Portland cement systems comprised of blends of calcium-aluminate cements[13,14] and magnesium (asbestos)-based systems[14].

This paper reports preliminary results on several super-critical cementitious systems evaluated after a short-term curing of 24 hours at 400°C and 25.5 MPa. The work was done in the frame of a joint international project focused on development of "sustainable geothermal well cement for challenging thermo-mechanical conditions" (Test-Cem[15]) under the umbrella of Cofund GEOTHERMICA.

2. MATERIALS AND METHODS

2.1 Samples Preparation and Testing

The tested formulations included high-temperature formulation of Portland cement modified with silica ($CaO-SiO_2$ system (S-1)), P_2O_5-Na_2O-CaO-Al_2O_3-SiO_2 – based systems with varied Al_2O_3/SiO_2 ratios (Al_2O_3/SiO_2 = 1.4 – system S-2, Al_2O_3/SiO_2 = 2.9 – system S-3), and P_2O_5-Na_2O-CaO-Al_2O_3-SiO_2-Fe_2O_3 (Al_2O_3/SiO_2 = 3.9 – S-4 system) phosphate system, Na_2O-CaO-Al_2O_3-SiO_2-MgO-Fe_2O_3 (Al_2O_3/SiO_2 = 0.43 – S-5 system) and Na_2O-CaO-Al_2O_3-SiO_2-MgO (Al_2O_3/SiO_2 = 0.15 – S-6 system) Mg-containing systems, and Na_2O-Al_2O_3-SiO_2 cement system (Al_2O_3/SiO_2 = 1.4 – S-7). OPC, class G, Dykerhoff North, cement in combination with silica flour was used as a reference cement. Calcium aluminate cements and alfa aluminum-oxide were supplied by Imerys Inc. Pozzolanic materials were obtained from Lafarge North America Inc and Imerys Inc. The blends were dry-mixed before adding water; the slurries were hand-mixed until getting a uniform suspension for about 2 minutes, then poured into 20 x 40 mm cylindrical molds and cured under hydrothermal conditions at 85°C (overnight) followed by overnight hydrothermal curing at 300°C and the final curing under the super-critical conditions at 400°C and pressure of 25.5 MPa in Parr autoclave reactor rated up to temperatures of 500°C and pressures of 34.46 MPa (5,000 psi). Inconel steel rapture disk rated to that pressure was used for the reported formulations. However, it should be noted, that some high alkalinity tested systems caused fast corrosion of rapture disks under super-critical conditions, which resulted in premature disk failures under the experimental pressures in less than 24 hr. Inconel steel disk replacement with corrosion resistant Hastelloy steel did not resolve this problem. These cement systems are not described in the current paper.

Samples' water-fillable porosities were measured by weighing the samples after the curing and after 3 days in a vacuum oven at 60°C. The porosity was calculated as (weight after curing - weight after vacuum oven)/ (weight after curing) x100%.

Electromechanical Instron System Model 5967 was used to obtain all mechanical properties. XRD (40 kV, 40 mA copper anode X-ray tube) was used for samples characterizations. The results of XRD tests were analyzed using PDF-4/Minerals 2021 database of International Center for Diffraction Data (ICDD). Additionally, JEOL 7600F Scanning Electron Microscope (SEM) image analyses coupled with EDX elemental composition survey were done for the typical spots on freshly broken samples. Cement samples were coated with silver to decrease the charging effects prior to the analyses.

3. RESULTS

3.1 Mechanical properties

Several potential cement chemistries of interest for super-critical environments were identified for the screening tests. The mechanical properties of some of them are shown in table 1. For most tested systems compressive strength decreased after the exposure to super-critical conditions. The two systems with the persisting strength were calcium-silicate system S-1 and magnesium-containing system S-6. Phosphate cements and magnesium S-5 system showed very high strength after the 300°C curing, which decreased after the 400°C exposure. The initial strength decrease is a known phenomenon for the phosphates cement and under hydrothermal conditions below super-critical, strength stabilization is generally observed after longer curing time[16]. The strength decrease for the tested cements was accompanied by the increase in toughness and decrease of Young's modulus suggesting less brittle cement after super-critical curing.

Table 1: Mechanical Properties of Tested Cement Systems

System (Al_2O_3/SiO_2)	Compressive strength, MPa (psi)		Toughness, Nmm/mm^3		Young's modulus, GPa (kpsi)	
	300°C	400°C	300°C	400°C	300°C	400°C
S-1 (0.04)	21 ± 2 (3100 ± 340)	24 ± 1 (3450 ± 160)	0.44 ± 0.12	0.39 ± 0.09	1.7 ± 0.1 (245 ± 15)	2.2 ± 0.2 (322 ± 29)
S-2 (1.4)	31 ± 4 (4560 ± 600)	23 ± 2 (3300 ± 250)	0.23 ± 0.12	0.48 ± 0.09	3.4 ± 0.2 (496 ± 34)	2.2 ± 0.4 (320 ± 57)
S-3 (2.9)	28 ± 2 (4000 ± 240)	24 ± 1(3400 ± 150)	0.38 ± 0.12	0.48 ± 0.11	2.7 ± 0.3 (396 ± 41)	2.2 ± 0.2 (316 ± 25)
S-4 (3.9)	35 ± 3 (5080 ± 390)	26 ± 2 (3700 ± 245)	0.18 ± 0.04	0.35 ± 0.05	4.0 ± 0.02 (585 ± 4)	3.7 ± 0.2 (542 ± 25)
S-5 (0.43)	28 ± 2 (4000 ± 300)	6.4 ± 0.7 (920 ± 100)	0.53 ±0.18	0.24 ± 0.1	2.3 ± 0.2 (334 ± 26)	0.6 ± 0.1 (95 ± 20)
S-6 (0.15)	10 ± 1 (1390 ± 95)	11 ± 2 (1550 ± 260)	0.22 ± 0.05	0.19 ± 0.06	0.7 ± 0.1 (105 ± 12)	1 ± 0.3 (145 ± 47)
S-7 (1.5)	-	8 ± 0.7 (1140 ± 100)	-	0.24 ± 0.02	-	0.65 ± 0.01 (94 ± 2)

3.2 Crystalline phase composition, microstructural development, water-fillable porosities

Figure 1 shows crystalline composition of the S-1 formulation after 300°C and 400°C curing. The patterns are similar, both are dominated by xonotlite peaks. Dehydrated calcium silicate wollastonite contributes some peaks to the pattern of 400°C-cured sample (2 theta 26.92, 36.37). Iron reacts at that temperature with formation of andradite (major peak at 2 theta of 32.97 and a new peak at 36.22). The main difference in the patterns is the disappearance or a strong decrease in the intensity of silica peaks after samples curing at 400°C (2 theta 25.42, 28.38, 49.45, 50.43). Calcium carbonate peaks also decrease (2 theta 24.44, the right shoulder between 29.24 and 29.68, 33.9, 40.23, 40.87, 44.89-45.45). Finally, sulphate mineral from cancrinite group, pitiglianoite, seem to decompose under super critical conditions (decrease of the peaks at 2 theta 27.5, 32.44, 33.92, 39.43, 42.47).

The morphological investigation confirms disappearance of silica (figure 2) – the large dark inclusions of silica on the left photomicrograph of the sample cured at 300°C disappear from the photomicrograph of the sample cured at 400°C (right). Long xonotlite crystals are clearly visible in the sample after the exposure to super-critical conditions. Significant part of the matrix is still amorphous after the short period curing of this study. The porosity of the system increased by 4.5% after the super-critical curing.

XRD patterns of S-2 phosphate system are shown in figure 3. The main phases for that system included dmisteinbergite (a polymorph of a stable high-temperature phase anorthite), bohmite, and hydroxyapatite. After the exposure to super-critical conditions the peaks of the mica group mineral margarite and a mineral related to muscovite phyllosilicate, paragonite, appeared in the XRD patterns. Additionally, small peaks of high-pressure, high-temperature calcium-aluminum-silicate donwilhelmsite were detected. Like in the case of S-1, silica peaks strongly decreased (2 theta 26.66). High-temperature zeolite analcime present after 300°C (low peak intensity) also decomposed under super-critical conditions.

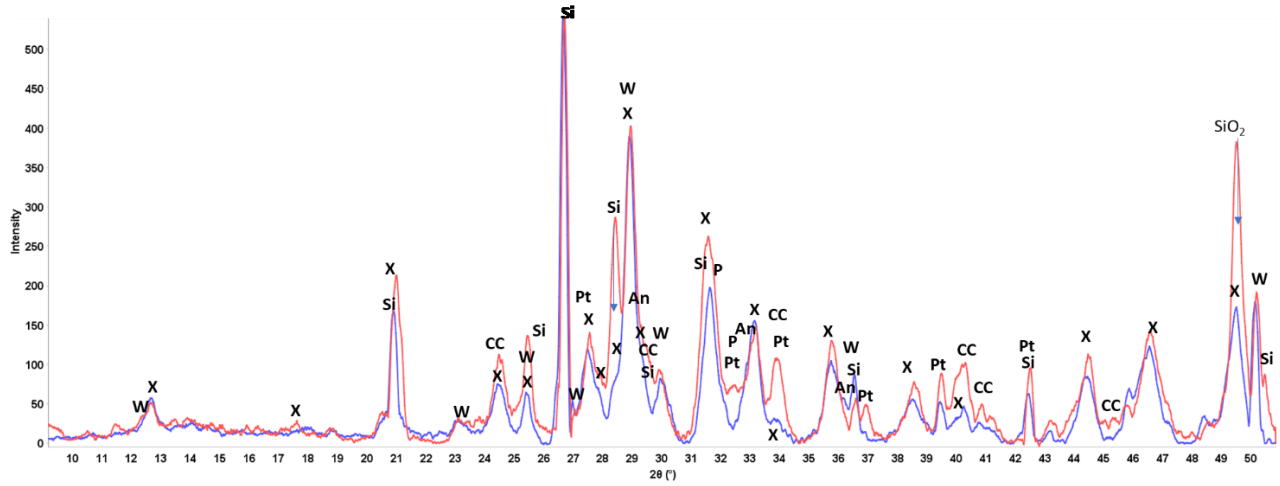

Figure 1: XRD patterns of $CaO\text{-}SiO_2$ (S-1) cement formulation after 300°C curing (red) and 400°C curing (blue). X - Xonotlite-Ma2bc (ICDD: 00-023-0125), Si – Silicon oxide (ICDD: 04-015-7165/01-077-8641/01-085-0797/01-0762980/01-089-8936/04-015-7167), W – Wollastonite-1A (ICDD: 00-042-0547), CC – Calcium Carbonate (ICDD: 01-085-6714/01-086-4274/04-013-7324), An – Andradite (ICDD: 01-084-8181), Pt – Pitiglianoite (ICDD: 04-014-5729), P – Portlandite (ICDD: 00-050-0008).

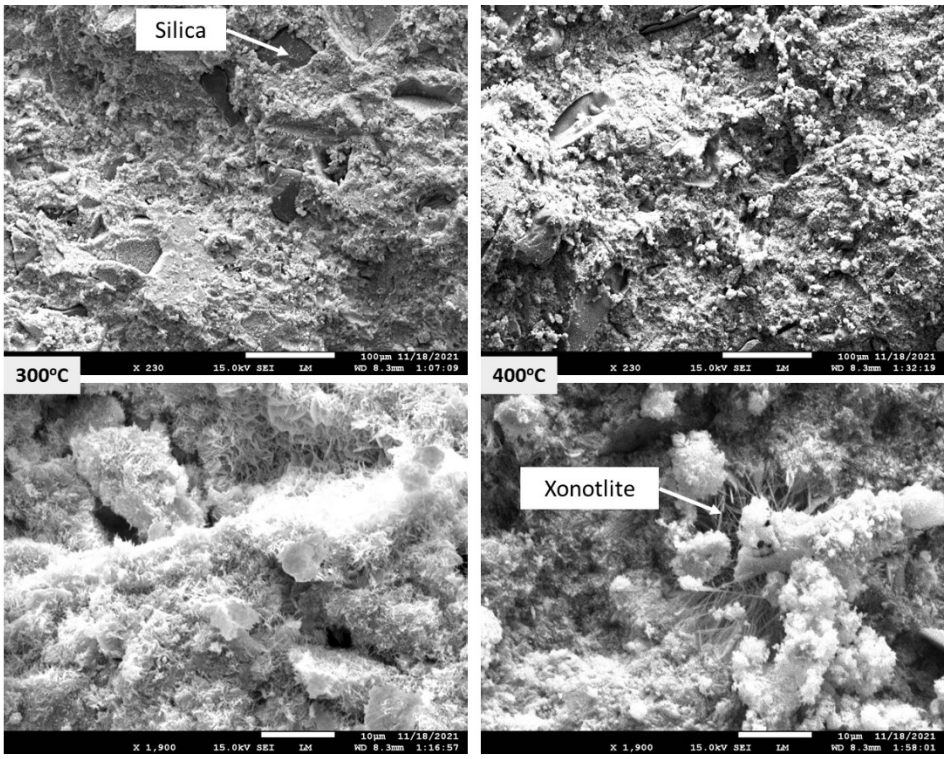

Figure 2: Photomicrographs of $CaO\text{-}SiO_2$ (S-1) cement formulation after 300°C curing and 400°C curing.

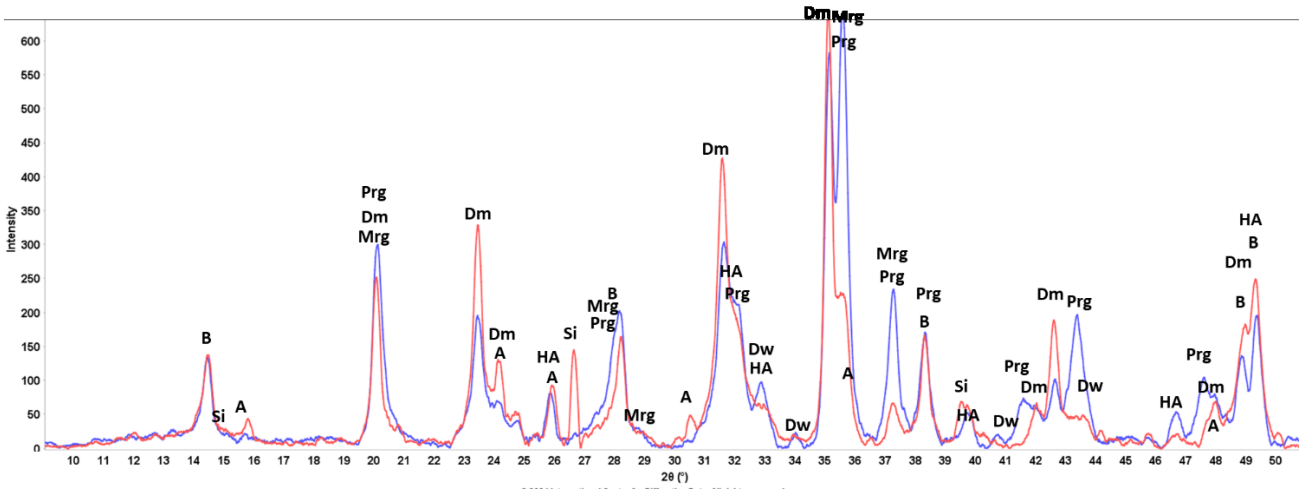

Figure 3: XRD patterns of P_2O_5-Na_2O-CaO-Al_2O_3-SiO_2 (S-2, $Al_2O_3/SiO_2 = 1.4$) cement formulation after 300°C curing (red) and 400°C curing (blue). Dm – Dmisteinbergite (ICDD: 00-051-0064), B – Bohmite (04-012-5050/01-088-2487), A – Analcime (ICDD: 01-070-1575), HA – Hydroxyapatite (ICDD: 01-074-9775), Prg – Paragonite-3T (ICDD: 01-083-2129), Mrg – Margarite 2M1 (ICDD: 04-013-3004), Si – Silicon oxide (ICDD: 01-088-2487), Dw – Donwilhelmsite (ICDD: 00-051-0093)

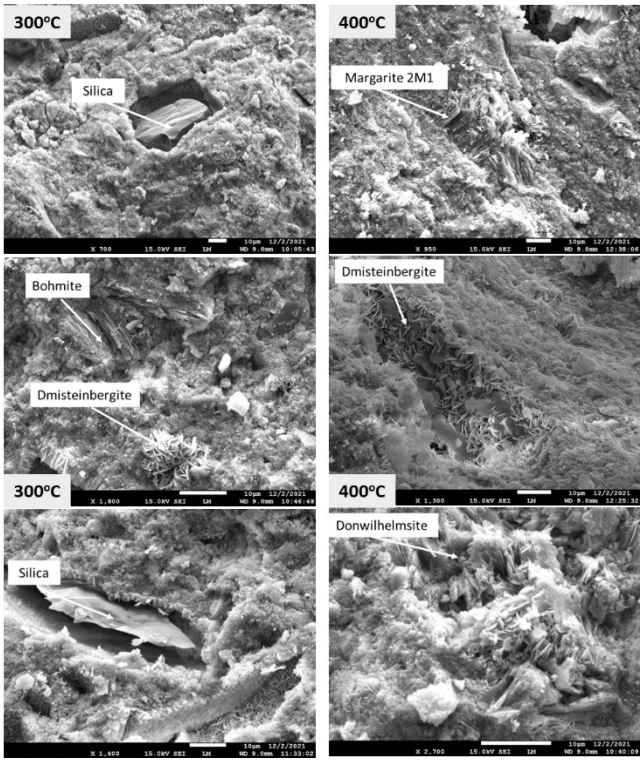

Figure 4: Photomicrographs of P_2O_5-Na_2O-CaO-Al_2O_3-SiO_2 (S-2, $Al_2O_3/SiO_2 = 1.4$) cement formulation after 300°C curing and 400°C curing.

Morphology of S-2 sample was mostly amorphous both after 300° and 400°C curing. Crystals of dmisteinbergite, bohmite, margarite, silica, and donwilhelmsite, identified by XRD analysis were seen in the matrix (figure 4). Big silica crystals clearly visible in the 300°C-cured sample were not present in the sample cured at 400°C. The porosity of this system increased by 3.0% after the super-critical curing.

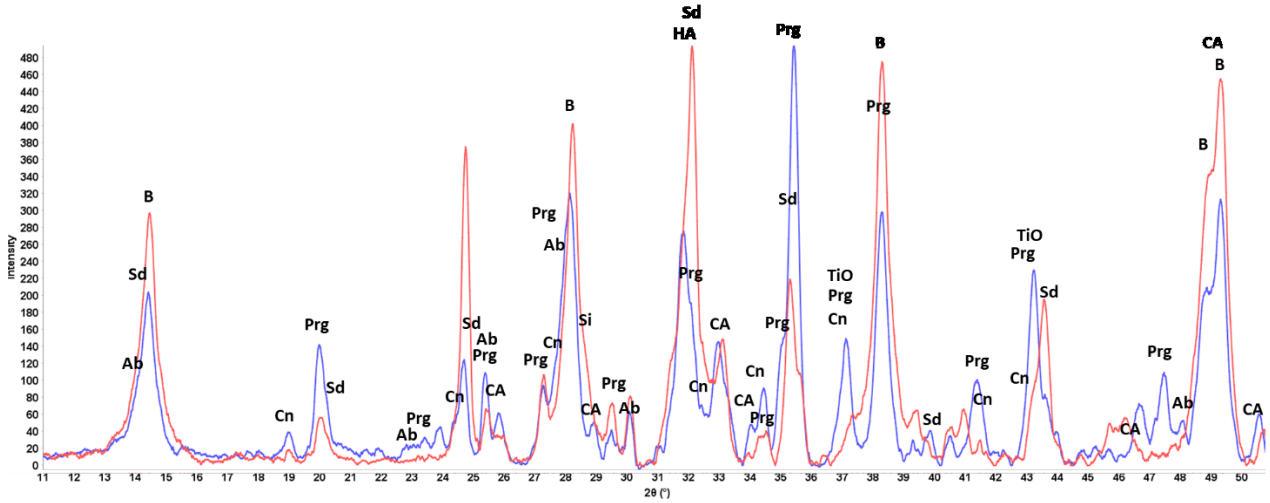

Figure 5: XRD patterns of P_2O_5-Na_2O-CaO-Al_2O_3-SiO_2 (S-3, $Al_2O_3/SiO_2 = 2.9$) cement formulation after 300°C curing (red) and 400°C curing (blue). B – Bohmite (ICDD: 04-014-2197), CA – Carbonated Apatite (ICDD: 04-012-6510), Sd – Sodalite (ICDD: 01-073-5298), Cn – Cancrinite (ICDD: 04-011-2738), HA – Hydroxyapatite (ICDD: 04-013-6655), Prg – Paragonite-3T (ICDD: 01-083-2129), Ab – Albite (00-009-0466).

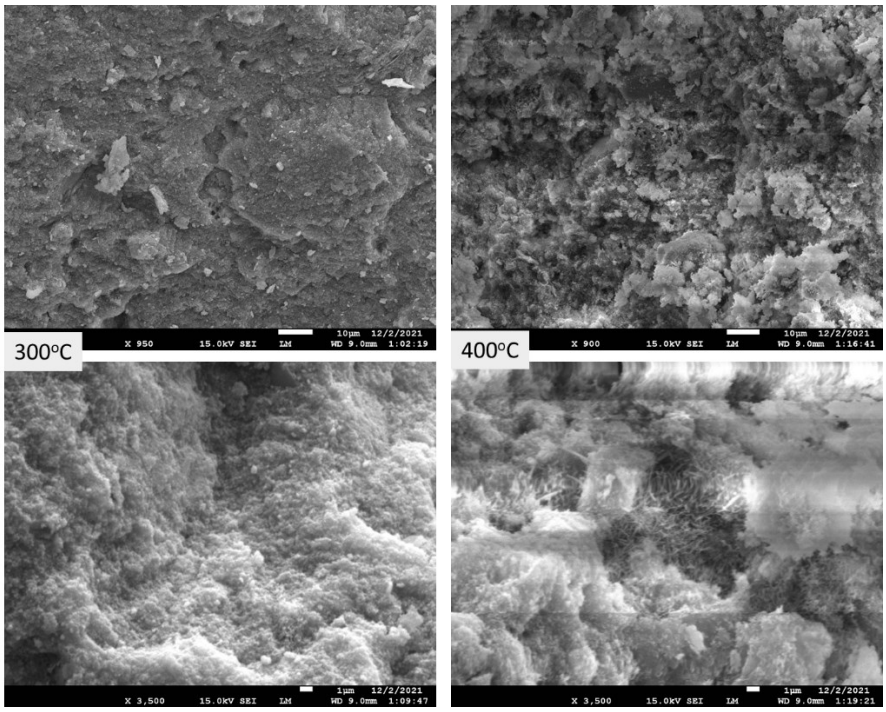

Figure 6: Photomicrographs of P_2O_5-Na_2O-CaO-Al_2O_3-SiO_2 (S-3, $Al_2O_3/SiO_2 = 2.9$) cement formulation after 300°C curing and 400°C curing.

When aluminum content increases in the P_2O_5-Na_2O-CaO-Al_2O_3-SiO_2 (S-3, $Al_2O_3/SiO_2 = 2.9$) the XRD pattern does not include anorthite-type minerals or zeolites after 300°C curing. It is dominated by apatite phases and bohmite. The peaks' intensities of these minerals decrease after the super-critical curing and like in the case of S-1 sample, paragonite peaks become predominant in the pattern. A feldspathoid group mineral cancrinite replaces sodalite and peaks of sodium-aluminum silicate, albite, appear in the pattern (figure 5). Matrix of the sample is very dense and mostly amorphous (figure 6). Small crystals of Al-rich bohmite are visible in the matrix in the bottom right photomicrograph of 400°C-cured sample. There was a very little increase in porosity of this system after the super-critical curing – 0.14%.

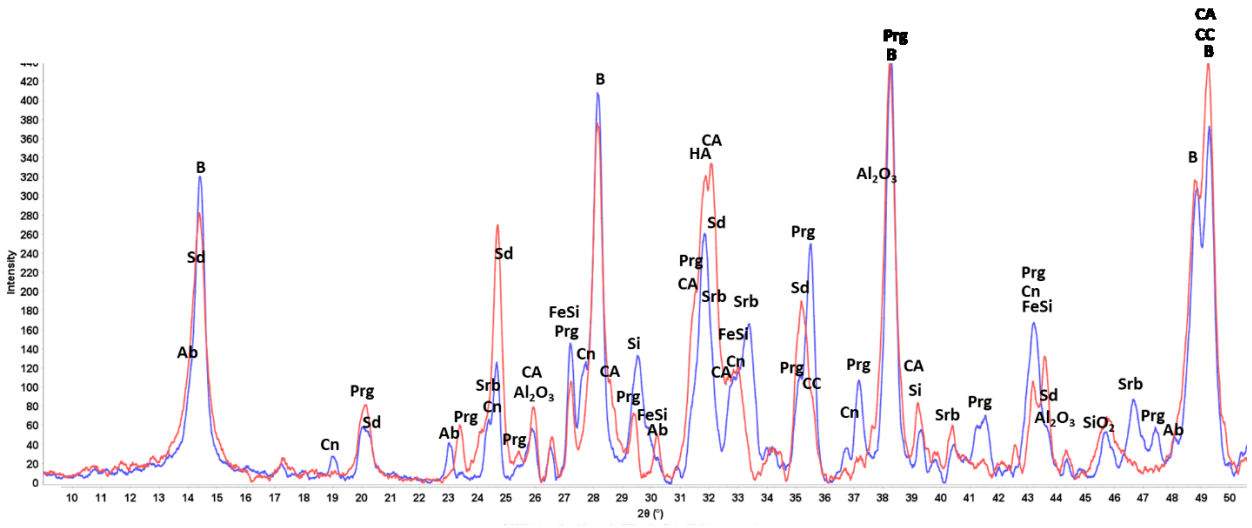

Figure 7: XRD patterns of P_2O_5-Na_2O-CaO-Al_2O_3-SiO_2-Fe_2O_3 (S-4, $Al_2O_3/SiO_2 = 3.9$) cement formulation after 300°C curing (red) and 400°C curing (blue). B – Bohmite (ICDD: 04-014-2197), HA – Hydroxylapatite (ICDD: 01-080-3243), CA – Carbonate apatite (ICDD: 01-072-9861), Sd – Sodalite (ICDD: 01-073-5298), Si – silicon oxide (ICDD: 04-008-8222), Prg – Paragonite-3T (ICDD: 01-083-2129), Ab – Albite (ICDD: 00-009-0466), Cn – Cancrinite (ICDD: 04-011-2738), CC – calcium carbonate (ICDD: 04-014-1681), Srb – Srebrodolskite (ICDD: 01-084-9445), FeSi – Asimowite ferrian (ICDD: 00-050-0088).

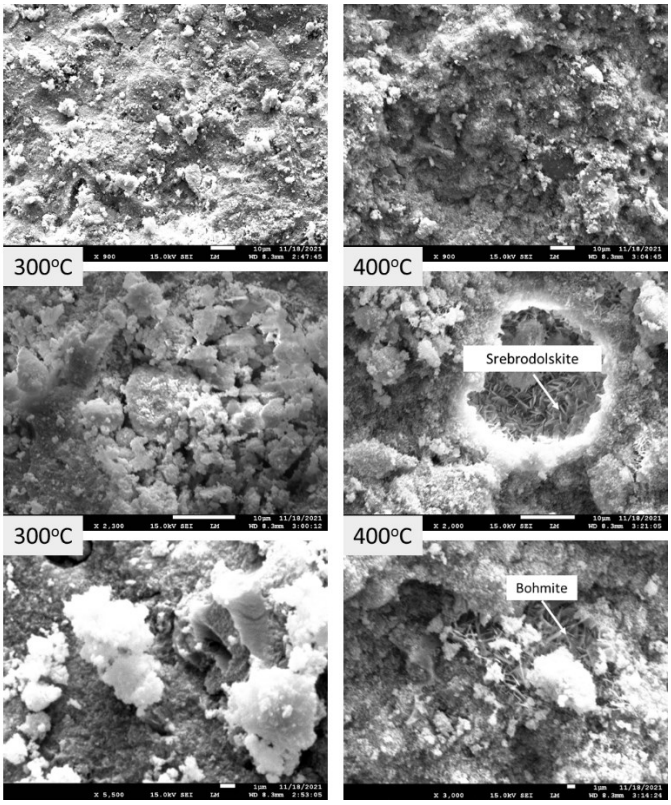

Figure 8: Photomicrographs of P_2O_5-Na_2O-CaO-Al_2O_3-SiO_2-Fe_2O_3 (S-4, $Al_2O_3/SiO_2 = 3.9$) cement formulation after 300°C curing and 400°C curing.

Further increase of aluminum content does not dramatically change the XRD patterns (figure 7, sample S-4). They are still dominated by apatite and bohmite. However, bohmite is stabilized by the higher aluminum presence and its peaks persist after the super-critical curing, while the peaks of apatite decrease in intensity like in the case of S-3 sample. Like for S-3 sample paragonite becomes an important phase after the super-critical curing and small albite peaks appear. Iron-containing minerals srebrodolskite and asimowite ferrian are present in the patterns of 400°C-cured sample for this system containing iron. Mostly amorphous matrix after 300°C curing remains amorphous after

the 400°C exposure (figure 8). But it is clearly less dense than that of S-3 sample. The porosity of S-4 increased by 3.1% after the super-critical curing.

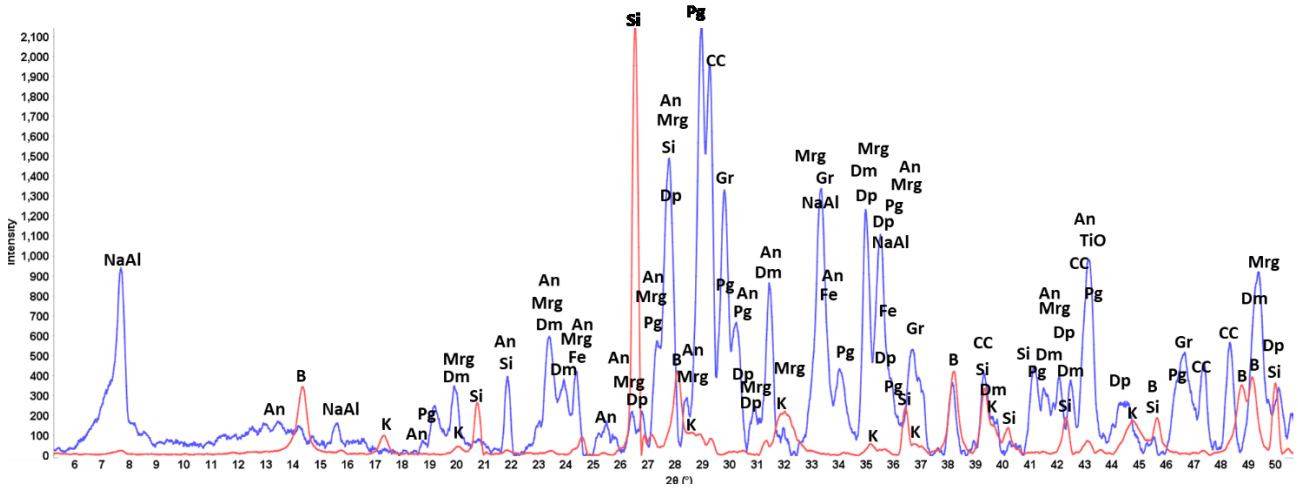

Figure 9: XRD patterns of Na_2O-CaO-Al_2O_3-SiO_2-MgO-Fe_2O_3 (S-5, Al_2O_3/SiO_2 = 0.43) cement formulation after 300°C curing (red) and 400°C curing (blue). Dm – Dmisteinbergite (ICDD: 00-051-0064), An – Anorthite Na-bearing (ICDD: 01-078-2330), Si – Silicon oxide (ICDD: 01-077-8623/01-075-8322), K – Katoite (ICDD: 01-074-2900/01-077-1713), B – Boehmite (ICDD: 04-017-4319), Gr – Grossular, Fe-bearing (ICDD: 01-076-0923), Dp – Diopside (ICDD: 01-085-2500), Pg – Pigeonite (ICDD: 01-071-0712), Mrg – Margarite-2M1 (ICDD: 01-076-0883), Fe – Hematite (ICDD: 01-080-5408), CC – Calcite (ICDD: 04-012-8072), NaAl – Sodium oxide aluminum oxide (ICDD: 01-076-0923).

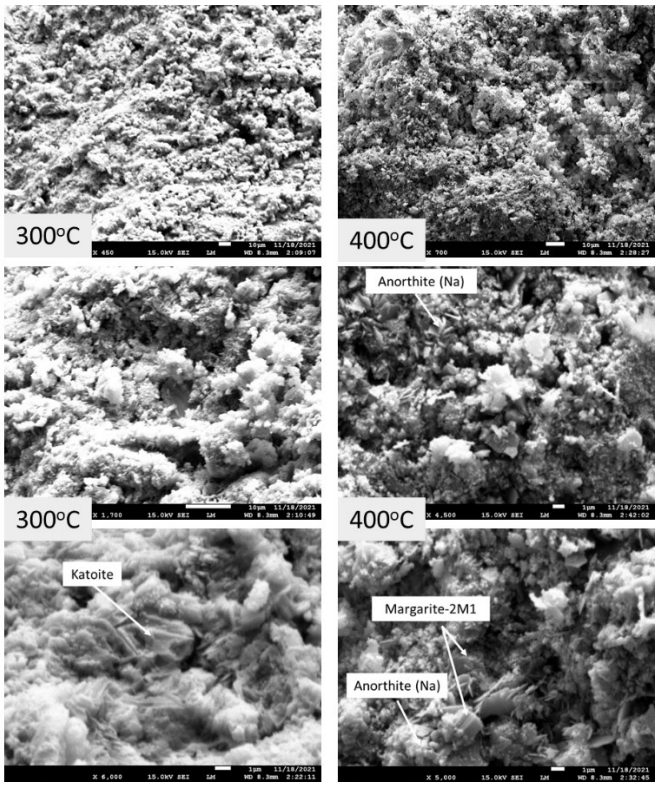

Figure 10: Photomicrographs of Na_2O-CaO-Al_2O_3-SiO_2-MgO-Fe_2O_3 (S-5, Al_2O_3/SiO_2 = 0.43) cement formulation after 300°C curing and 400°C curing.

Magnesium-containing system S-5 was mostly amorphous after the 300°C curing (figures 9 and 10). The major peaks in the XRD pattern belong to crystalline silica (figure 9). There were also peaks of bohmite and katoite. Crystals of katoite were also visible in the photomicrograph of the sample (figure 10). A complex XRD pattern was obtained for the sample cured at 400°C. Silica, bohmite, and katoite peaks dramatically decreased while a combination of high-temperature phases including paragonite, margarite, anorthite, and

dmisteinbergite appeared. If these phases were present in other earlier described systems, diopside and grossular were specific to S-5. The photomicrographs confirmed the findings of XRD with the visible crystals of anorthite and margarite (figure 10). The porosity of the system increased by 10.4%.

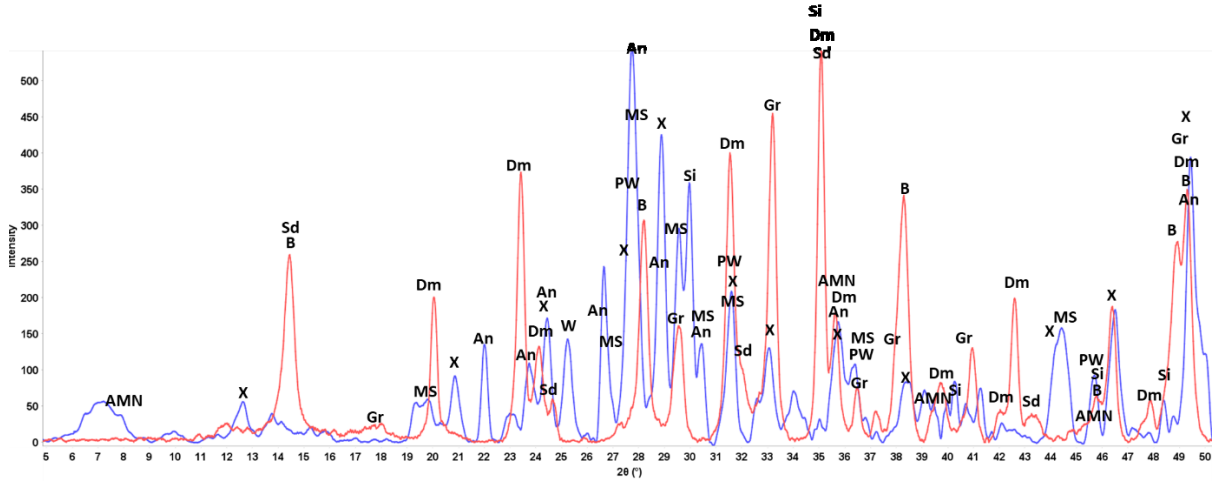

Figure 11: XRD patterns of Na_2O-CaO-Al_2O_3-SiO_2-MgO (S-6, Al_2O_3/SiO_2 = 0.15) cement formulation after 300°C curing (red) and 400°C curing (blue). Dm – Dmisteinbergite (ICDD: 04-011-6236), Si – Silicon oxide (ICDD: 01-080-2157/01-086-4007), B – Bohmite (ICDD: 04-010-5683), Gr – Grossular, Fe-bearing (ICDD: 01-076-0923/00-003-0801), Ge – Gehlenite (ICDD: 04-014-7820), Sd – Sodalite (ICDD: 00-011-0401), X – Xonotlite-2M (ICDD: 01-076-1846), An – Anorthite (ICDD: 01-074-2539), MS – Magnesium Silicate (ICDD: 01-076-6764/04-008-5467), PW – Pseudowollastonite (ICDD: 04-011-3072), W – Wollastonite (ICDD: 01-076-1846), AMN – Aluminum Magnesium Sodium oxide (ICDD: 01-073-9552).

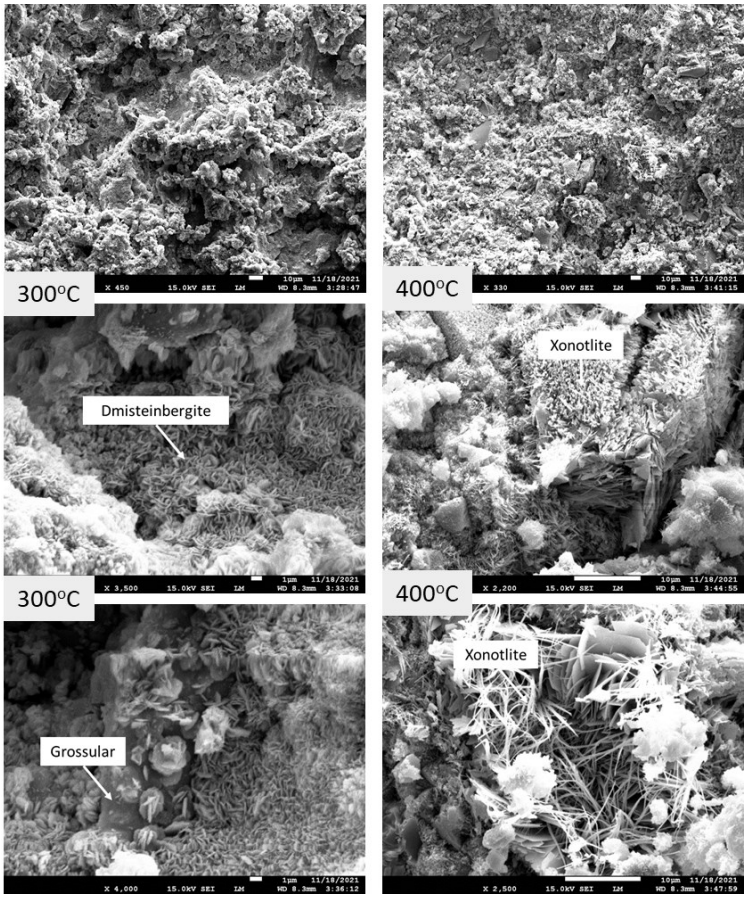

Figure 12: Photomicrographs of Na_2O-CaO-Al_2O_3-SiO_2-MgO (S-6, Al_2O_3/SiO_2 = 0.15) cement formulation after 300°C curing and 400°C curing.

The system Na_2O-CaO-Al_2O_3-SiO_2-MgO (S-6, Al_2O_3/SiO_2 = 0.15), with lower aluminum content formed dmisteinbergite, grossular and bohmite after 300°C curing (figures 11 and 12). Exposure to super-critical conditions resulted in crystallization of xonotlite, magnesium silicate, transformation of dmisteinbergite to anorthite, and decomposition of bohmite. Peaks of wollastonite and pseudo wollastonite showed up in the XRD patterns. Aluminum magnesium sodium oxide that gives peaks at low angle may be formed during cooling the autoclave before samples removal. The increase in the system porosity was 9.9%.

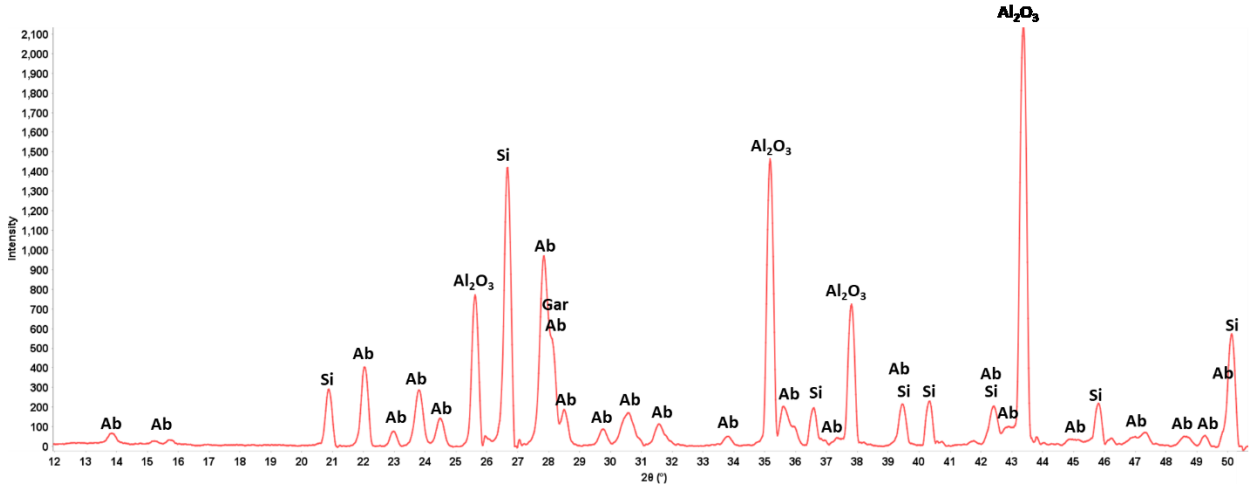

Figure 13: XRD patterns of Na_2O-Al_2O_3-SiO_2 (S-7, Al_2O_3/SiO_2 = 1.5) cement formulation after 400°C curing (blue). Al_2O_3 – corundum (ICDD: 01-073-6190), Si – Quartz (ICDD: 01-075-8320), Ab – Albite (ICDD: 01-089-6430), Gar – Garronite (ICDD: 00-070-0072).

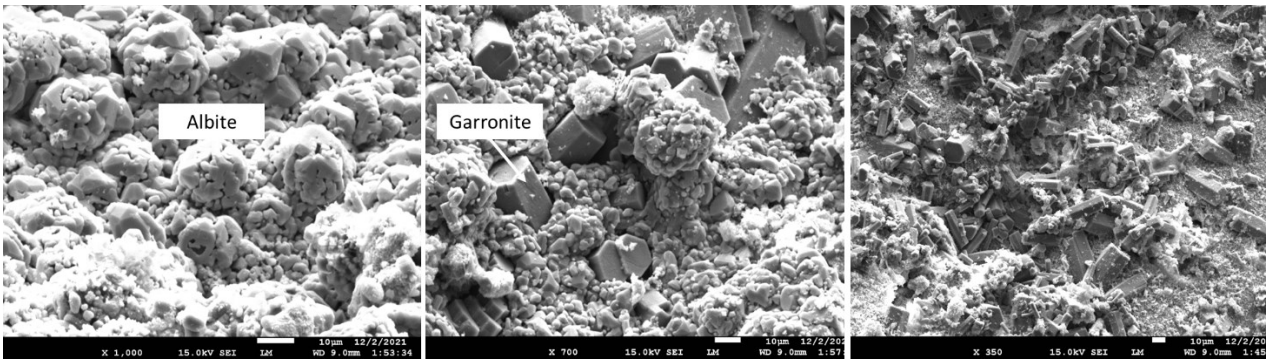

Figure 14: Photomicrographs of Na_2O- Al_2O_3-SiO_2 (S-7, Al_2O_3/SiO_2 = 1.5) cement formulation after 400°C curing.

A simple system of Na_2O-Al_2O_3-SiO_2 (S-7, Al_2O_3/SiO_2 = 1.5) was tested after 400°C (figure 13, 14). Crystalline composition of the sample was made of sodium aluminum silicate albite, sodium garronite ($Na_6(Al_6Si_{10}O_{32})$ ·7.3 H_2O) and non-reacted aluminum oxide. These crystals were densely packed in partially amorphous matrix (figure 14).

3. DISCUSSION AND CONCLUSIONS

Super-critical conditions present very special environments for materials to survive. Significant pitting corrosion of rapture disk made of steel alloys (Inconel and Hastelloy) occurred during the experiments at 400°C and 25.5 MPa under hydrothermal conditions. The corrosion rate was higher when highly alkaline cement samples were tested. For cement formulations with the pH of pore water around 13 Hastelloy rapture disk corroded within less than 18 hours of the experiment. However, the corrosion occurred even for the samples with pore water pH between 8 and 12. Figure 15 shows the Inconel rapture disk images after 72 hrs under supercritical conditions in the presence of cement samples.

Forty-two samples (sample volume 6 mL) were tested in an autoclave (volume 1.8 L) in four separate runs at 400°C, 25.5MPa. All cement samples were alkaline with the pH of pore solution ranging between ~9 and 12. After completion of the tests, the Inconel rapture disk was removed and analyzed with the 3D optical microscope. The image in figure 15 reveals strong pitting corrosion (silver spots) detected over the whole surface of the disk. The profile of the deepest corrosion spot under the photograph indicates that the corrosion penetrated through more than 80% of the disk thickness. In addition to the difficulties of testing cements under the super critical conditions, casing corrosion should be carefully considered for super-critical geothermal wells.

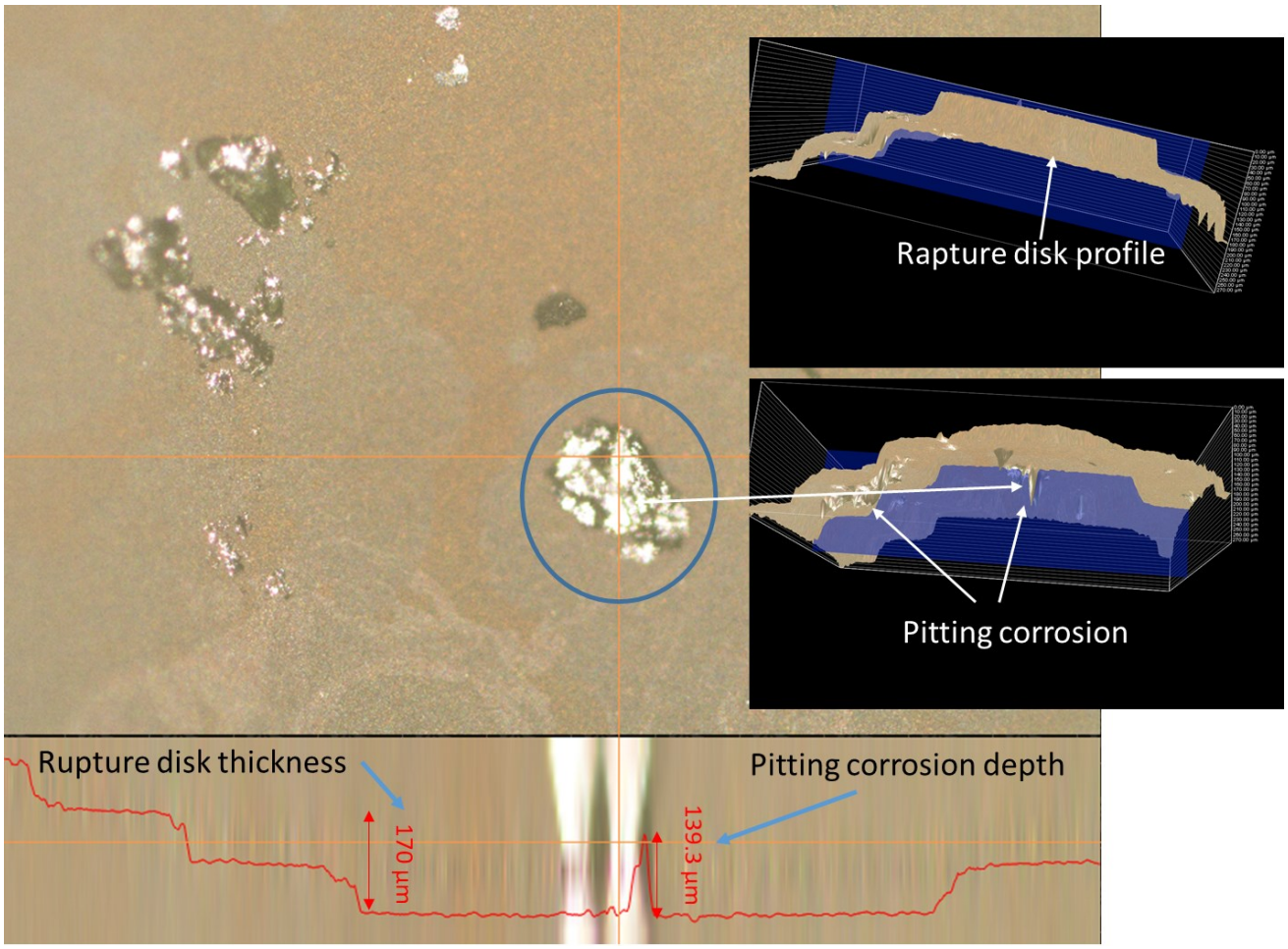

Figure 15: Surface of Inconel rapture disk after 72 hrs in an autoclave with cement samples at 400°C, 25.5 MPa hydrothermal environment. The bright spots are locations of pitting corrosion seen all over the disk. The red line shows profile of the deepest corrosion spot. The black images on the right are the 3D photographs of the disk (two views) with the downward corrosion peak nearly penetrating through the thickness of the disk.

In $CaO\text{-}SiO_2$ system (S-1) the major crystalline phase, xonotlite, persisted after the short-term curing under super-critical conditions, changing its morphology to longer needles. Crystalline silica, carbonate, and sulfate phases were not stable disappearing from the XRD patterns of the 400°C-cured sample. Mechanical properties of the system were not compromised in a short term with both compressive strength and Young's modulus being higher for the super-critical sample (24 MPa at 400°C vs. 21 MPa at 300°C). However, morphological changes resulted in the increase in system's porosity by more than 4%.

In the $P_2O_5\text{-}Na_2O\text{-}CaO\text{-}Al_2O_3\text{-}SiO_2$ systems (S-2, S-3, S-4) phosphate-containing apatite phases, partially decomposed under super-critical conditions been replaced by the high-temperature stable phase, paragonite. At low Al_2O_3/SiO_2 = 1.4 feldspathoid calcium-aluminum-silicate, dmisteinbergite, and high-temperature zeolite, analcime, formed after 300°C along with bohmite and hydroxyapatite. Dmisteinbergite and analcime did not form in S-3 and S-4 systems with higher Al_2O_3/SiO_2 ratios of 2.9 and 3.9 respectively. Bohmite persisted through 400°C curing, cancrinite, albite, srebrodolskite (Fe-bearing mineral in S-4) were present in samples with Al_2O_3/SiO_2 = 2.9 and 3.9. Higher aluminum content stabilized both bohmite and apatite phases as seen by the intensity of their peaks at the patterns of 400°C-cured samples. The matrix of these systems was for the most part amorphous after high-temperature curing. After the short-term curing phosphate systems developed very high strength after 300°C (31MPa for S-2, 28MPa for S-3, and 35MPa for S-4), The strength decrease after the exposure to super critical conditions was more important for the systems with the higher initial compressive strength (26% for S-2 and S-4 vs.24% for S-3). S-3 system with the intermediate Al_2O_3/SiO_2 of 2.9 possessed the higher toughness of 0.38 that further increased to 0.48 Nmm/mm^3 after the 400°C curing. As mentioned above, strength-stabilization is expected for phosphate cements after the initial strength decrease. The porosity increase was less important for the tested phosphate systems than for the calcium-silicate S-1. S-2 and S-4 porosity increase was around 3% while S-3 showed only 0.14% of the porosity increase after the super-critical curing.

Magnesium-containing systems S-5 and S-6 underwent significant crystalline phase changes during the super-critical curing. This was especially visible for S-5 (Al_2O_3/SiO_2 = 0.43) that started with silica, bohmite, and some katoite (low peaks' intensities) after the 300°C curing. After the super-critical exposure, the XRD patterns were very complex. For the higher Al_2O_3/SiO_2 (0.43) they were dominated by feldspathoid minerals dmisteinbergite and its polymorph anorthite, mica-type mineral margarite, grossular, and Mg-containing mineral diopside. Anorthite and diopside were shown to have desirable cementitious properties under super-critical conditions of 400°C and

pressures of up to MPa (10,000 psi) after curing times of several months[14]. For the system with the lower Al_2O_3/SiO_2 of 0.15 xonotlite, anorthite, wollastonite, and magnesium silicate were among the dominant phases. Grossular and dmisteinbergite peaks that were major after 300°C greatly diminished after the 400°C curing. Unlike for other systems bohmite is not stable at 400°C in MgO-systems with low Al_2O_3/SiO_2 ratio. The matrix of these samples was more crystalline than for the phosphate systems. The dramatic changes in crystallinity for the S-5 system during the super-critical curing resulted in striking decrease in mechanical properties from 28MPa after 300°C curing to 6.4MPa after 400°C exposure. The strength of the S-5 system, on the other hand, persisted through super-critical curing (10MPa before 400°C exposure and 11MPa after the exposure). Intergrown crystalline microstructures apparently served to enhance the strength of the S-5 sample. Nevertheless, both systems experienced significant increase in porosity, which was 10.4% for S-5 and 9.9% for S-6.

The Na_2O-Al_2O_3-SiO_2 (S-7, Al_2O_3/SiO_2 = 1.5) system formed highly crystalline matrix of high-temperature stable mineral albite, zeolite garronite with some non-reacted silica and aluminum oxide.

It should be noted that some changes in the tested systems could have taken place during the cooling of the autoclaves from super critical conditions.

Among the tested systems phosphate system with the intermediate Al_2O_3/SiO_2 ratio of 2.9 showed the most promise as new geothermal cement for super-critical conditions. It demonstrated acceptable and persisting mechanical properties, crystalline phase development and morphological composition, as well as very little porosity increase after the 400°C curing (0.14%). Although Mg-containing systems developed high initial compressive strength and formed high-temperature stable crystalline phases, such as anorthite and diopside, dramatic phase changes caused strength decrease for the system with lower aluminum content and significant increase in porosity (around 10%) in both systems after the super-critical curing. Further long-term testing is needed to fully evaluate the real potential of the selected formulations.

4. ACKNOWLEDGEMETS

This project has been subsidized through the Cofund GEOTHERMICA by DoE (the USA, GTO EERE under the auspices of the US DOE, Washington, DC, under contract No. DE-AC02-98CH 10886), RVO NL (the Netherlands), and the Research Council of Norway. Contributions from our partners Equinor (Norway), EBN (The Netherlands), Imerys (France), and CURISTEC (France) are greatly acknowledged. Research was carried out in part at the Center for Functional Nanomaterials, Brookhaven National Laboratory, which is supported by the US Department of Energy, Office of Basic Energy Sciences, under Contract No. DE-SC0012704.

5. REFERENCES

1. Hill, L. B. Superhot Rock Geothermal A Vision for Zero-Carbon Energy "Everywhere". *CATF* Available at: https://www.catf.us/wp-content/uploads/2021/09/CATF_SuperhotRockGeothermal_Report.pdf.

2. Garrison, G., Uddenberg, M., Petty, S., Watz, J. & Hill, L. B. Resource Potential of SuperHot Rock. in *GRC Transactions, Vol 44* (2020).

3. Elders, W. A., Frioleifsson, G. O. & Pálsson, B. Iceland deep drilling project: The first well, IDDP-1, drilled into magma. *Geothermics* 49, 1 (2014).

4. Bonneville, A., Cladouhos, T., Petty, S., Schults, A. & Sorlie, C. Toward Super Hot EGS: The Newberry Deep Drilling Project. in *GRC Transactions, Vol. 42* (2018).

5. Asanuma, H., Muraoka, H., Tsuchiya, N. & Ito, H. The concept of the Japan Beyond-Brittle project (JBBP) to develop EGS reservoirs in ductile zones. in *GRC Transactions, Vol 36* (2012).

6. Asanuma, H., Soma, N., Tsuchiya, N., Kajiwara, T. & Yamada, S. Concept of development of supercritical geothermal resources in Japan. in *International Conference on Geothermal Energy in Taiwan* (2015).

7. Muraoka, H., Asanuma, H., Tsuchiya, N., Ito, T, Mogi, T. & Ito, H. The Japan Beyond-Brittle project. *Sci. Drill* **17**, (2014).

8. Reinsch, T. *et al.* Utilizing supercritical geothermal systems : a review of past ventures and ongoing research activities. *Geotherm. Energy* 1–25 (2017). doi:10.1186/s40517-017-0075-y

9. GEMex website. Available at: http://www.gemex-h2020.eu/index.php?lang=en.

10. Bruhn, H. GEMex: cooperation Europe–Mexico for the development of unconventional geothermal systems. *Tagungsband, Der Geotherm.* (2017).

11. Lopez Hernandez, A. *et al.* GEMex-cooperación Mxico-Europa para la investigación de sistemas geotérmicos mejorados y sistemas geotérmicos supercalientes. *GEOS* (2016).

12. Bignall, G. & Carey, B. A deep (5km?) geothermal science drilling project for the Taupo Volcanic Zone-who wants in? in *New Zealand Geothermal Workshop Proceedings* (2011).

13. Sakuma, S., Naganawa, S., Sato, T., Ito, T. & Yoshida, Y. Evaluation of High-Temperature Well Cement for Supercritical

Geothermal Drilling. in *GRC Transactions, Vol. 45* 268–283 (2021).

14. Roy, D. M. New High Temperature Cementing Materials for Geothermal Wells: Stability and Properties. (1980).

15. Sustainable Geothermal Well Cement for Challenging Thermo-Mechanical Conditions. (2021). Available at: https://www.bnl.gov/test-cem/.

16. Sugama, T., Weber, L. & Brother, L. Sodium-polyphosphate-modified fly ash/calcium aluminate blend cement: durability in wet, harsh geothermal environments. *Mater. Lett.* 44, 45–53 (2000).